Journal of Earth Science, *Vol. 28*, *No. 4*, *p. 709–718*, *August 2017* *ISSN 1674-487X*
Printed in China
DOI: 10.1007/s12583-017-0749-1

Sequential and Simultaneous Joint Inversion of Resistivity and IP Sounding Data Using Particle Swarm Optimization

Yi'an Cui*, Zhixue Chen, Xiaoxiong Zhu, Haifei Liu, Jianxin Liu
School of Geosciences and Info-Physics, *Central South University*, *Changsha* 410083, *China*; *Hunan Key Laboratory of Nonferrous Resources and Geological Hazard Detection*, *Central South University*, *Changsha* 410083, *China*; *Key Laboratory of Metallogenic Prediction of Nonferrous Metals of Ministry of Education*, *Central South University*, *Changsha* 410083, *China*
Yi'an Cui: http://orcid.org/0000-0002-4811-642X

ABSTRACT: In order to interpret the vertical electrical sounding data more reliably and effectively in the case of lacking proper priori information, two inverse schemes are proposed to invert combined resistivity and induced polarization data by using particle swarm optimization technique. Based on the computational formula of induced polarization, the inversion for chargeability/polarizability data can be transformed into inverting equivalent resistivity data. Then, the inversion for combined data can be decomposed into two procedures: inverting resistivity data and inverting equivalent resistivity data. A sequential inversion scheme is presented to run the two procedures sequentially. Contrast to the sequential scheme, a simultaneous one is proposed to invert resistivity and induced polarization data simultaneously. Both the sequential and simultaneous schemes are performed via centered-progressive particle swarm optimization algorithm for more exploratory purpose. Numerical experiments show that both the designed inversion algorithms can invert resistivity and induced polarization data successfully with fast convergence and high accuracy, even performed in a large search space. The inverse results are comparable to the results from generalized linear method. As an approximate importance sampler, the particle swarm optimization based algorithm can provide posterior analysis conveniently. We employ the posterior probability distributions of inverted model parameters to evaluate the performance and uncertainty of inversion. The posterior analysis and further field data testing show that the proposed inversion algorithms perform good sampling of the equivalence region and make sure that the global optimum can locate in the high probability areas.
KEY WORDS: inversion, particle swarm optimization, resistivity, induced polarization.

0 INTRODUCTION

Both direct current (DC) resistivity methods and induced polarization (IP) methods are very important branches of exploration geophysics. DC resistivity methods are commonly used in minerals prospecting, groundwater exploration, and civil engineering applications (Ye et al., 2015; Tang et al., 2011; Zhu et al., 2011; Chandra et al., 2010). IP methods also have been regarded as an efficient means to locate groundwater and contaminant plumes (Atekwana et al., 2015; Gallas et al., 2011; Fernández-Martínez et al., 2010a). In fact, the resistivity data and IP data can be observed at the same time in a field survey, and the two data sets are complementary to each other (Niwas and Gupta, 2011). In some applications, both of the two data sets are used in data interpretation to reduce the uncertainties and ambiguities (Johnson et al., 2010; Veeken et al., 2009). Although the resistivity data and IP data can be measured simultaneously with the same array in the field, the inversions of observed data, in general, are implemented separately. In this paper, we propose a novel inversion to invert the resistivity and IP data simultaneously.

Inversion plays a very important role in DC resistivity and IP data interpretation. Like most geophysical inversions, quantitative estimation of the parameters of a layered geo-electric structure from observed DC resistivity and IP data always is a nonlinear inverse problem (Niwas and Gupta, 2011). Because the global minimum of these problems is located at the bottom of a narrow, elongated valley with almost null gradients, global optimization methods are a good selection due to their probabilistic nature (Fernández-Martínez et al., 2010b). Global optimization methods are becoming increasingly popular in the recent years. The simulated annealing and genetic algorithm are widely used in the geophysical inversion (Sen Mrinal and Stoffa, 2013). More recently, swarm intelligence algorithm has attracted much attention in many fields. The main reason is that swarm intelligence algorithms do not need any global model or central control to perform with. One of the most used swarm intelligence algorithms is particle swarm optimization (PSO). The PSO originally proposed by Kennedy and Eberhart (1995), is a population based optimization algorithm by mimicking the

*Corresponding author: cuiyian@csu.edu.cn

Manuscript received July 25, 2016.
Manuscript accepted December 27, 2016.

social behavior of individuals while searching for food as a member of the swarm. PSO algorithm can parallel search for solution in a given model space. The algorithm is simple and easy to be implemented, and has been widely applied in many fields, such as image processing and electrical engineering problems. Shaw and Srivastava (2007) used the concept of PSO to invert VES, IP and magneto telluric data. Santos and El-Kaliouby (2010) presented a comparative study on the use of PSO method and other local optimization methods in the joint inversion of Time Domain Electromagnetic and direct current resistivity data. Santos (2010) and Cui et al. (2016) also successfully used PSO to invert the self-potential data of idealized bodies' anomalies. Fernández-Martínez et al. (2012, 2010a, b) applied PSO algorithms for many geophysical inverse problems viz., the streaming-potential, the vertical electrical sounding (VES), and the reservoir characterization. They established that PSO has the advantages of being a very fast sampler yielding good balance between exploration and convergence except time consuming. Some other recent applications of PSO to invert different geophysical data include self potential (Pekşen et al., 2011) and Rayleigh wave dispersion (Song et al., 2012).

In this paper, a joint inversion for resistivity and IP sounding data based on PSO algorithm is presented. Firstly, a sequential version, called sequential PSO (Se-PSO), is introduced. In the Se-PSO inversion, the resistivity data is inverted as the first stage. Only after getting satisfactory results from the first stage, the IP data is inverted. Then, a simultaneous inversion, called simultaneous PSO (Si-PSO) inversion, is discussed to invert both the resistivity and IP data at the same stage.

1 METHODS SCHEMES

After acquiring the resistivity and IP sounding data, joint inversion is considered an effect way to characterize the depth variation of subsurface structure distribution.

1.1 Forward Modeling of VES

The forward problem use the same VES model as introduced by Fernández-Martínez et al. (2010b). The geo-electric structure is assumed to be horizontally stratified, characterized by the resistivity ρ_i, chargeability η_i and the thicknesses h_i of ith electrical layer. The model can be represented by a vector

$$m = (\rho_1, \rho_2, \cdots \rho_n, \eta_1, \eta_2, \cdots \eta_n, h_1, h_2 \cdots h_{n-1}) \tag{1}$$

m belongs to a $3n-1$ dimensional vector space M, where n is the number of layers.

To solve the forward problem, one assume that m is known and computes the corresponding apparent resistivity $\rho_a(d, m)$ and apparent chargeability $\eta_a(d, m)$ at the surface. The mathematical expression of the relationship between m and $\rho_a(d, m)$ is given by Koefoed (1979) as follows

$$\rho_a(d,m) = \rho_1 + d^2 \int_0^\infty (H_1(\lambda,m) - \rho_1) \cdot J_1(\lambda d) \lambda d\lambda \tag{2}$$

where d is the distance between the current electrodes, J_1 is the first order Bessel function, H_1 is the resistivity transform kernel for the first layer, and λ is the integration variable. The use of the Pekeris relations allows computation of the resistivity transform kernel H_1 for each layer, recursively from the bottom to the surface, following the formula

$$H_n(\lambda) = \rho_n \tag{3}$$

$$H_i(\lambda) = (H_{i+1} + \rho_i \cdot th(\lambda h_i)) / (1 + H_{i+1} \cdot th(\lambda h_i)/\rho_i) \tag{4}$$

where $H_i(\lambda)$ is the resistivity transform for the ith layer, $th(\lambda h_i)$ is the hyperbolic tangent function. The above formula proceeds recursively upward until H_1 is determined for the surface layer. Then the Eq. (2) is calculated.

The chargeability of earth materials is essentially an electrochemical effect caused by many factors. If ground is chargeable, it responds as if resistivity was a complex quantity. Apparent chargeability, the most commonly used IP parameter, can be defined as (Seigel, 1959)

$$\eta_a(d,m) = (\rho_a^e(d,m) - \rho_a(d,m) / \rho_a^e(d,m)) \tag{5}$$

where $\rho_a^e(d,m)$ is the apparent resistivity at the presence of polarization in the medium.

In a given model, the values of resistivity ρ_i and chargeability η_i of ith geo-electrical layer are available. Then, the equivalent resistivity ρ_i^e of each layer is computed by the function as

$$\rho_i^e = \rho_i / (1 - \eta_i) \tag{6}$$

After getting the equivalent resistivity values of each layer, the corresponding equivalent apparent resistivity $\rho_a^e(d,m)$ at the surface is calculated as the same way as $\rho_a(d, m)$ mentioned above. Finally, the corresponding apparent chargeability $\eta_a(d,m)$ is computed by Formula (5).

1.2 Sequential and Simultaneous Inversion Schemes

The inversion scheme is designed to estimate a series of parameters of model m through the observed resistivity and chargeability sounding data sets,

$$\rho_a^o(d) = (\rho_a^o(d_1), \rho_a^o(d_2), \cdots \rho_a^o(d_{nd})) \tag{7}$$

$$\eta_a^o(d) = (\eta_a^o(d_1), \eta_a^o(d_2), \cdots \eta_a^o(d_{nd})) \tag{8}$$

for an array $d=(d_1, d_2, \cdots, d_{nd})$ of the distance between the current electrodes, aimed to minimize a scalar cost function, relative misfit. The relative misfit is used to quantify the distance between observations and predictions

$$rmf(m) = \left\| \rho_a^o(d) - \rho_a(d,m) \right\|_2 \Big/ \left\| \rho_a^o(d) \right\|_2 \tag{9}$$

$$cmf(m) = \left\| \eta_a^o(d) - \eta_a(d,m) \right\|_2 \Big/ \left\| \eta_a^o(d) \right\|_2 \tag{10}$$

where $rmf(m)$ is the relative misfit of resistivity and $cmf(m)$ is the relative misfit of chargeability.

1.2.1 Sequential inversion

Generally, the inversion for combined resistivity and IP sounding data consists of two stages. The resistivity and thickness data are inverted firstly. Then the chargeability data are inverted by using the resistivity structure obtained from the inversion of the resistivity data. That is usually called sequential inversion as a kind of joint inversion (Masson et al., 2012). In this scheme, the procedure of inversion can be described as follows.

Step 1. Initialize the parameters (ρ_i, h_i) of the geo-electrical model.

Step 2. Use a inversion method, such as the PSO algorithm which will be introduced in the next section, to invert the resistivity data, and get the reliable resistivity distribution (ρ_i, h_i) via minimized *rmf*(*m*).

Step 3. Initialize the chargeability η_i of *i*th layer for the geo-electrical model.

Step 4. Calculate the equivalent resistivity ρ_i^e of *i*th layer through Eq. (6) by using the initialized chargeability η_i in Step 3 and the inverted resistivity ρ_i in Step 2.

Step 5. Compute the equivalent apparent resistivity $\rho_a^e(d,m)$ at the surface by the forward modeling mentioned above.

Step 6. Calculate the corresponding apparent chargeability $\eta_a(d, m)$ by Eq. (5) and the relative misfit *cmf*(*m*) by Eq. (10).

Step 7. Evaluate the relative misfit *cmf*(*m*), adjust the initialized chargeability η_i and repeat Step 4 to Step 7 until a desired *cmf*(*m*) is achieved.

1.2.2 Simultaneous inversion

In contrast to the separate inversion, the simultaneous inversion takes a strategy to invert the resistivity, thickness and chargeability data simultaneously. The procedure of simultaneous inversion can be described as follows.

Step 1. Initialize the parameters (ρ_i, η_i, h_i) of geo-electrical model.

Step 2. Calculate the equivalent resistivity ρ_i^e of *i*th layer through Eq. (6) by using the initialized ρ_i and η_i of *i*th layer.

Step 3. Calculate the apparent resistivity $\rho_a(d, m)$ using parameters (ρ_i, h_i) and the equivalent apparent resistivity $\rho_a^e(d,m)$ using parameters (ρ_i^e, h_i).

Step 4. Transform the measured data $\rho_a^o(d)$ and $\eta_a^o(d)$ into the equivalent apparent resistivity $\rho_a^{oe}(d)$ through Eq. (6).

Step 5. Calculate the relative misfit *rcmf*(*m*) to quantify the distance between observations and computations

$$rcmf(m) = w_1 \cdot rmf(m) + w_2 \cdot cmf(m) \tag{11}$$

where w_1 and w_2 are constants to weight the relative misfit of resistivity and chargeability, and the sum of w_1 and w_2 constant equals to 1.

Step 6. Evaluate the relative misfit *rcmf*(*m*), adjust initialized parameters (ρ_i, η_i, h_i) and repeat Step 2 to Step 5 until a desired minimized *rcmf*(*m*) is achieved.

2 PSO ALGORITHM

Obviously, both the sequential and simultaneous inversions are nonlinear and over-determined. These inverse problems are challenges due to their ill-posed characteristics. It is caused by the data noises and incomplete data coverage. To solve this kind of problems, PSO algorithm is recommend as a powerful global search method by many researchers (Fernández-Martínez et al., 2012, 2010a, b; Pekşen et al., 2011; Santos and El-Kaliouby, 2010; Shaw and Srivastava, 2007).

In PSO, each particle is treated as a point in a multi-dimensional space, initialized without any volume and mass. Each particle represents a potential solution to a related optimal problem. The performance of particles is evaluated by a pre-set fitness function. Each particle moves according to its own experience and its companions' experience in the solution space. The direction and distance of the movement depends on a velocity variable. Through iterative searching, particles track the most optimal current particle and find the optimal solution.

In the PSO algorithm for geophysical inversion, each geophysical model is called a particle and described as a vector whose length is the number of degrees of freedom. The search space of the geophysical model is defined as

$$l_j \le x_{ji} \le u_j \ (1 \le j \le n,\ 1 \le i \le N_{\text{size}}) \tag{12}$$

where l_j and u_j are the lower and upper limits for the *j*th parameter of the *i*th geophysical model, *n* is the number of parameters in the inverse problem, N_{size} is the size of the swarm. Each particle has its own velocity $V_i(k)$ and position $X_i(k)$ in the search space. The velocities provide the parameter perturbations to find the solution of the geophysical problem. The velocity of each particle *i* at each *k*th iteration is a function of three components.

$$V_i(k+1)=\omega V_i(k)+r_1 a_g(g(k)-X_i(k))+r_2 a_l(l_i(k)-X_i(k)) \tag{13}$$

The first term on the right of Eq. (13) is the inertia term, given by the old velocity vector of a particle weighted by a real constant ω called inertia. The second is social learning term, which is the difference between the particle's current position and the best global position $g(k)$ found in the swarm. The parameter a_g is the global acceleration constants. The third is the cognitive learning term, which is the difference between the particle's current position and the particle's personal historical best position $l_i(k)$ found so far. The parameter a_l is the local acceleration constants. Both r_1 and r_2 are vectors of random numbers uniformly distributed on (0, 1) to weight the global and local acceleration constants.

After each iteration, the velocity and position of each particle are updated and the (*k*+1)th position of particle *i* is represented as

$$X_i(k+1)=X_i(k)+V_i(k+1) \tag{14}$$

The algorithm mentioned above is the most general form known as the basic PSO. To perform the sequential and simultaneous inversion for the sounding data, the basic PSO algorithm may be a simple choice. There are several successful applications via the basic PSO algorithm (Trelea, 2003; Clerc and Kennedy, 2002). However, PSO can be used as set of algorithms for exploitation or exploration. In geophysical inversion, exploitative algorithm is used to looking for a unique global minimum while explorative one is suitable to sample low-misfit region in the model space (Fernández-Martínez et al., 2010a). So, an explorative version of PSO is more suitable to the VES case because its low misfit models are located in a valley with very low gradients (Fernández-Martínez et al., 2010b). A centered-progressive PSO, or CP-PSO, was presented to the geophysical community as one of a whole family of PSO algorithms (Fernández-Martínez and García-Gonzalo, 2009; Fernández-Martínez et al., 2008). The main difference between CP-PSO and basic PSO is the way they update the positions and the velocities of particles. The basic PSO updates the velocity and then the position. However, CP-PSO updates the velocity and the position at the same time. This characteristic make CP-PSO has a more exploratory capability.

In CP-PSO, the position of each particle is updated as

$$X_i(k+1)=X_i(k)+V_i(k) \quad (15)$$

Fernández-Martínez et al. (2010a, b) proved that explorative inversions give better results for the VES case. So, in order to test the inversion schemes for the resistivity and IP sounding data, the detailed algorithms are designed for the sequential and simultaneous inversion respectively based on the CP-PSO algorithm. The sequential inversion algorithm (Se-PSO) is shown in Fig. 1 and the simultaneous one (Si-PSO) is shown in Fig. 2.

There are some parameters needed to be set to run the PSO algorithms. The number of particles N_{size} and the maximum iteration number K_{max} are basic parameters of a PSO algorithm. The number of particles gives the population size of particle swarm. In this paper, the population size of 100 is used in PSO algorithm, and the maximum iteration number is set to be 100. Both are determined after evaluating the performance in experiments.

Tuning the inertia weight ω, global acceleration constants a_g and local acceleration constants a_l can make PSO works well and provide a balance between exploration and exploitation and control the PSO convergence. But there are no magic tuning points that exist. The best parameters may be picked up close to the second order stability region (Fernández-Martínez et al., 2010b). The CP-PSO version itself has good exploration and convergence

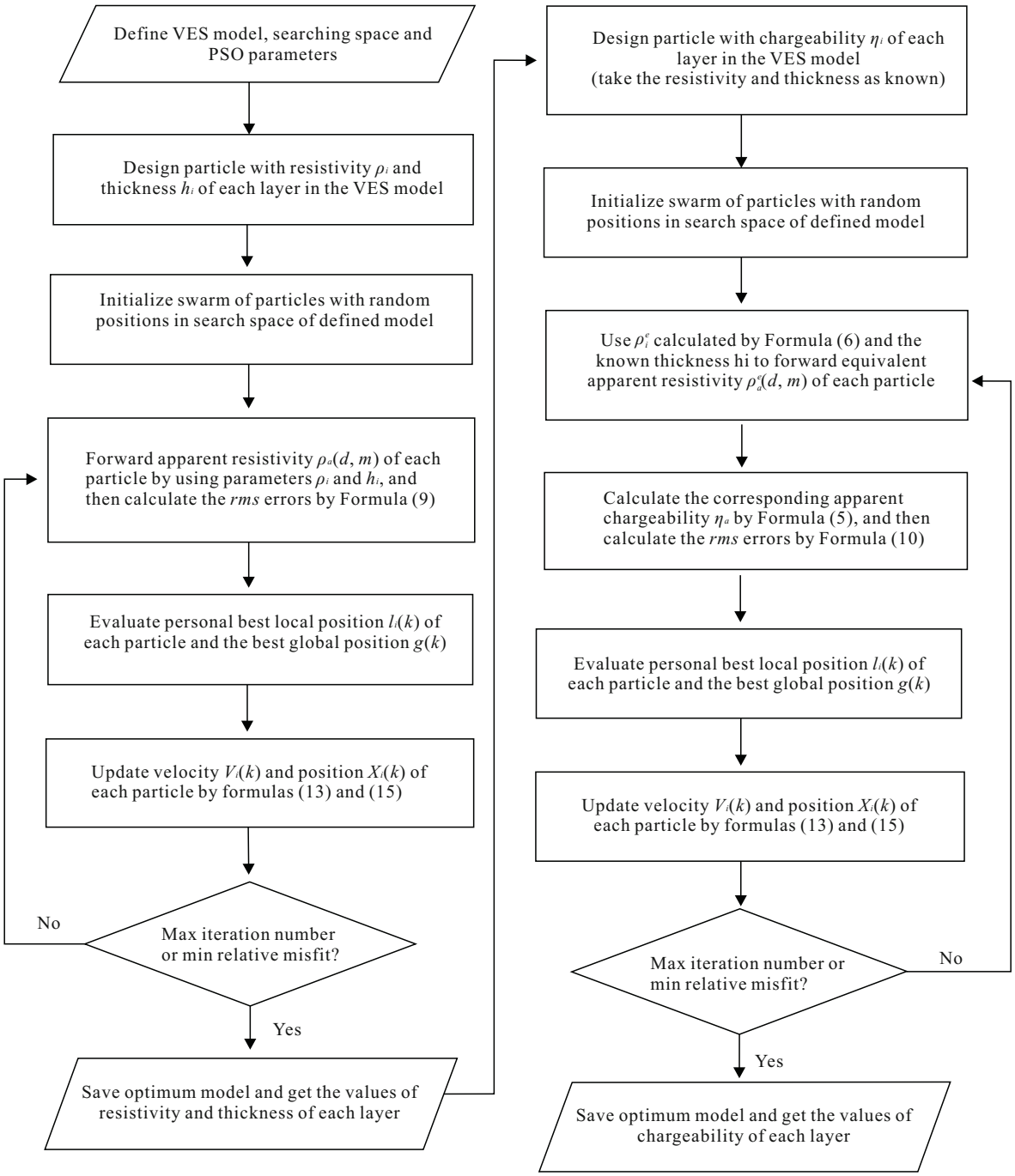

Figure 1. Se-PSO algorithm flow diagram of inversion for combined resistivity and IP data.

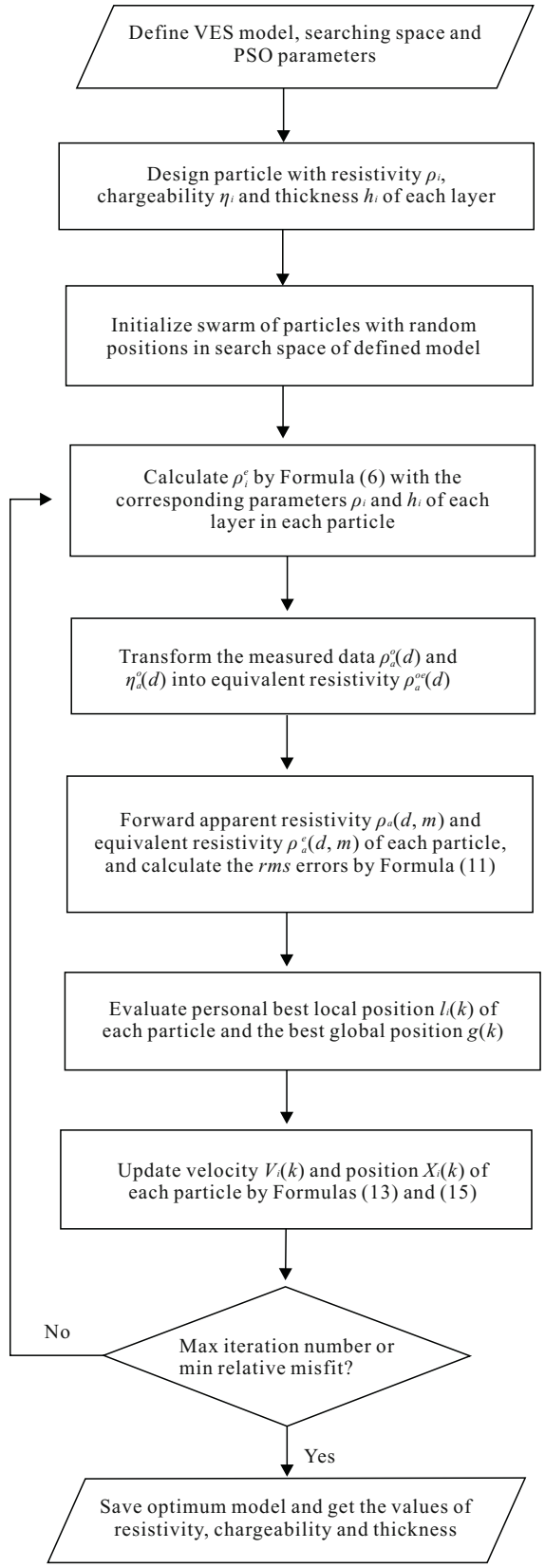

Figure 2. Si-PSO algorithm flow diagram of inversion for combined resistivity and IP data.

rate for VES inverse problem. So, for simplicity, we directly use the (ω, a_l, a_g) values as (0.545, 3.27, 1.64) chosen from literature (Fernández-Martínez et al., 2010b).

In Si-PSO algorithm, the relative misfit *rcmf*(m) is a linear combination of *rmf*(m) and *cmf*(m). The coefficients, w_1 and w_2, are used to balance the contribution of resistivity data and chargeability data in the inversion. In this paper, both w_1 and w_2 are set to be a same value 0.5 for considering the same importance of the two data sets.

3 SYNTHETIC EXAMPLE

To examine the performance of inversion, the Se-PSO and Si-PSO algorithm are tested by synthetic data. In order to facilitate the comparison and analysis, the synthetic data are generated from a three-layered geo-electrical model used by Shaw and Srivastava (2007). But we used a wider search space for inversion (Table 1). To simulate the observed field data from a noisy measurement, a random noise of 5% of the apparent resistivity values and 10% of the apparent chargeability values are added respectively to the synthetic data. The *rms* relative error of resistivity and chargeability are 6.8% and 5.8%, respectively.

Figure 3 shows the results of synthetic data testing. Figure 3a shows the match between noisy synthetic data and the predicted resistivity data from the models estimated by Se-PSO and Si-PSO algorithms. Figure 3b shows the match of chargeability data. For comparing, the results from generalized linear inverse method are given in the figure. The test shows that both Se-PSO and Si-PSO inversion algorithms have good performance in inverting synthetic data and are tolerant to the noises.

Figure 4 shows the variation of the relative error with iteration. The Se-PSO reaches the region of low misfit before 30 iterations for the resistivity inversion, and less than 10 iterations for the chargeability inversion. For the Si-PSO algorithm, the convergence rate is slow and the low-misfit region is reached after 70 iterations. This is caused by a higher dimension space involved in the inversion of the resistivity and chargeability data simultaneously. On the other hand, that means the Si-PSO have more exploitability. It can effectively avoid getting into local optimization too quickly.

Fernández-Martínez et al. (2012, 2010a) have demonstrated that PSO is an approximate importance sampler. So, we can draw histograms of inverted model parameters to measure the uncertainty of inversion. The uncertainty analysis is performed by making into account the particles that have been

Table 1 True parameter values and search space used in the VES model

Parameter	True value	Search space	
		Minimum	Maximum
ρ_1 (Ω·m)	2 500.0	10.0	5 000.0
ρ_2 (Ω·m)	100.0	10.0	5 000.0
ρ_3 (Ω·m)	300.0	10.0	5 000.0
h_1 (m)	1.5	1.0	50.0
h_2 (m)	25.0	1.0	50.0
η_1 (ms)	9.0	1.0	90.0
η_2 (ms)	4.5	1.0	90.0
η_3 (ms)	45.0	1.0	90.0

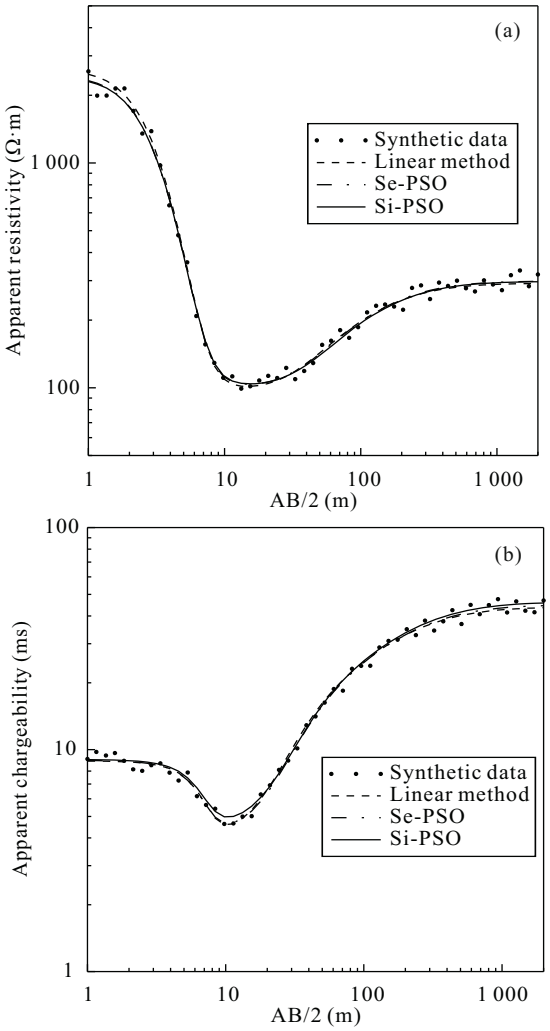

Figure 3. Match between noisy synthetic data and the predicted data. (a) The predicted resistivity data from models estimated from inversions using linear method, Se-PSO, and Si-PSO. (b) The predicted chargeability data from models estimated from inversions using linear method, Se-PSO, and Si-PSO.

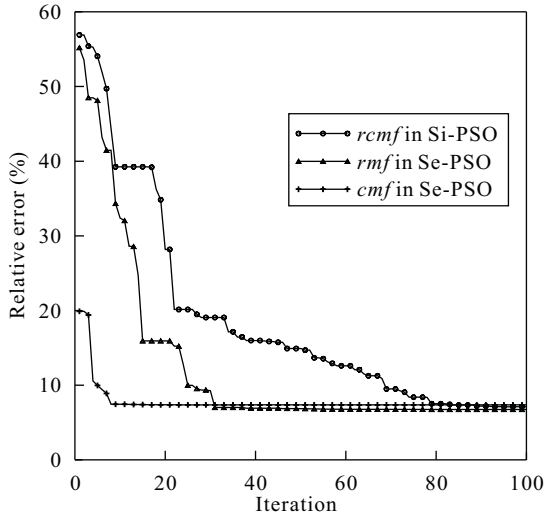

Figure 4. Variation of relative error with iteration.

collected on a low misfit region less than 15% relative error.

Figure 5 shows the histogram reconstruction of model parameters inverted by Se-PSO and Si-PSO, respectively. The frequency distribution of the model parameters can give valuable information with respect to the model parameter determination and identification. As shown in the figures, the inverse algorithms perform good posterior sampling of the equivalence region. That means the global optimum should locate in the high probability areas. Contrast to Fig. 5, there are wider histogram distributions in Fig. 6. That indicates the Si-PSO has more nonlinear character and more exploratory capability to search the model space more thoroughly.

To evaluate the robustness of the algorithms further, synthetic noise added data are generated from a five-layered geo-electrical model (ρ_1=2 500 Ω·m, η_1=9 ms, h_1=1.5 m; ρ_2=100 Ω·m, η_2=4.5 ms, h_2=5 m; ρ_3=1 500 Ω·m, η_3=20 ms, h_3=15 m; ρ_4=300 Ω·m, η_4=15 ms, h_4=25 m; ρ_5=2 000 Ω·m, η_4=45 ms) also have been tested. Figure 7 shows the results of testing. Figure 7a shows that the match between synthetic data and the predicted resistivity data from the models estimated by Se-PSO and Si-PSO algorithms. Figure 7b shows the match of chargeability data. The test shows that even in a more sophisticated case, the PSO inversion algorithms also have good performance. In contrast, the regular linear method can provide the similar results only when a carefully selected initial model was given.

4 FIELD EXAMPLE

To further evaluate the performance of Se-PSO and Si-PSO inversion algorithm, we test these algorithms with field data collected from Arufu, Benue, Nigeria. In this field, geological and geophysical studies have been carried out to locate mineral veins. And several sites are selected to conduct vertical electrical sounding with Schlumberger array. Both apparent resistivity data and polarizability data in forms of Percent Frequency Effect (PFE) were measured. The geological information indicates that there are 3 main formations in the sounding range. From the top to the bottom, these are the Quaternary packing clasolite, ferruginous breccia, basalt and silicarenite. From outcrop physical measurements, we obtain the resistivity and PFE variation range as shown in Table 2. Based on the geophysical and geological information, we employ a three-layer VES model to interpret the observed sounding data. Figure 8 shows the observed field data and the predicted data from the best models inverted by generalized linear inverse method, Se-PSO algorithm, and Si-PSO algorithm. As shown in the figure (see in Fig. 8a), all predicted resistivity data match the field data very well. The detailed values of inverted best models are shown in Table 2. In regards of resistivity and formation thickness, the inverted results coincide with the actual situations very well. But the inverted results of PFE data are not satisfactory (see in Fig. 8b). The reasons may include the existence of volume polarization effect, the coupling effect of sounding with Schlumberger array, and other complicated causes.

5 CONCLUSION

We have proposed a sequential inversion scheme and a simultaneous one to invert combined resistivity and IP sounding data. The PSO algorithm, especially exploratory version, is

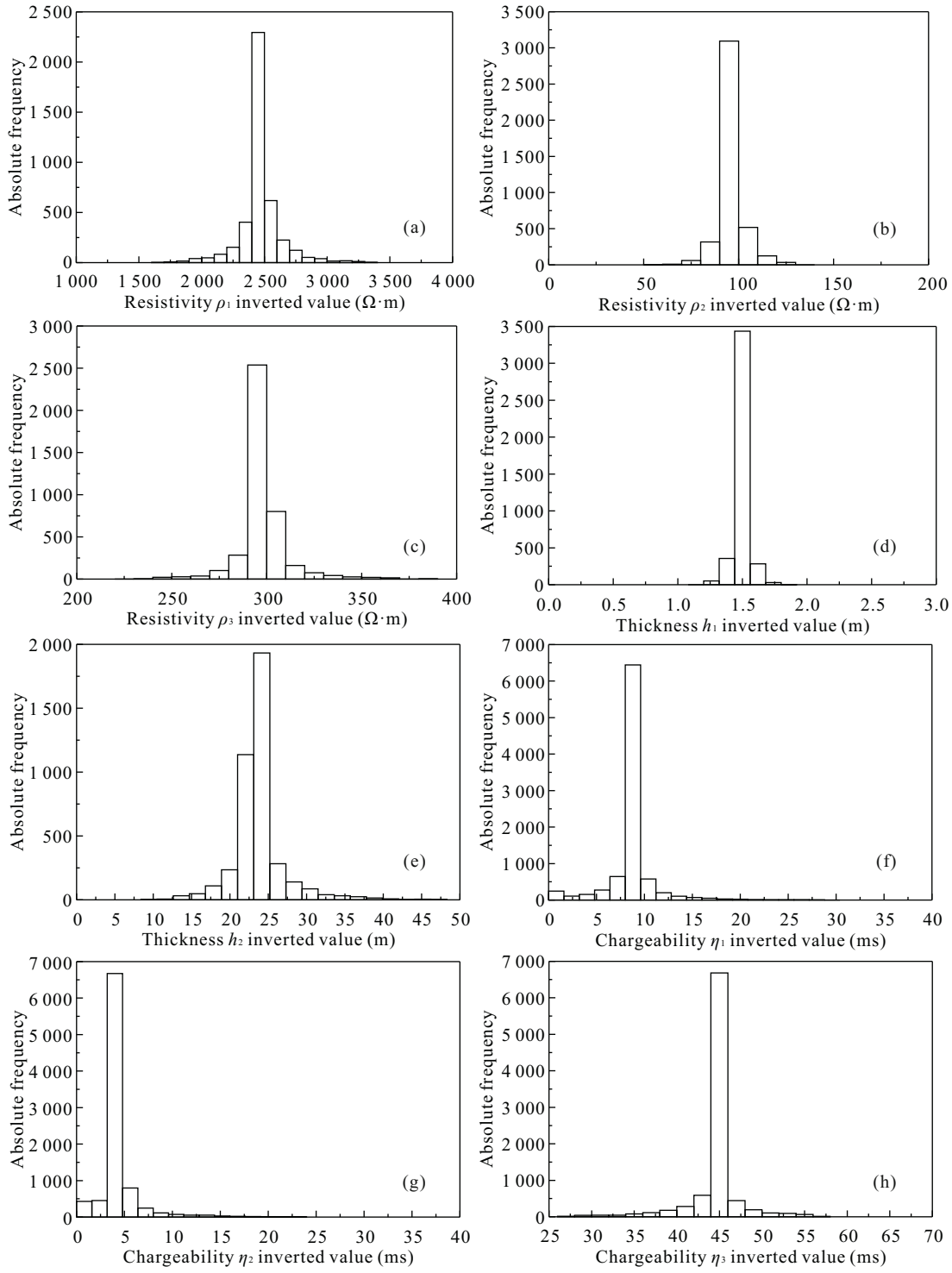

Figure 5. Histogram of inverted values ρ_1 (a), ρ_2 (b), ρ_3 (c), h_1 (d), h_2 (e), η_1 (f), η_2 (g) and η_3 (h) from Se-PSO inversion.

Table 2 Parameter values of inverted models and specimens testing results

Formation	Value of resistivity (Ω·m)				Value of PFE (%)			
	Specimens	G-linear	Se-PSO	Si-PSO	Specimens	G-linear	Se-PSO	Si-PSO
Quaternary clasolite	4 000–6 000	5 349	5 262	5 223	1.7–3.8	3.2	3.1	2.8
Ferruginous breccia	100–300	193	191	190	1.06–5.2	5.5	2.3	3.0
Basalt silicarenite	1 000–3 000	1 704	1 711	1 699	0.6–2.9	3.2	3.3	1.7

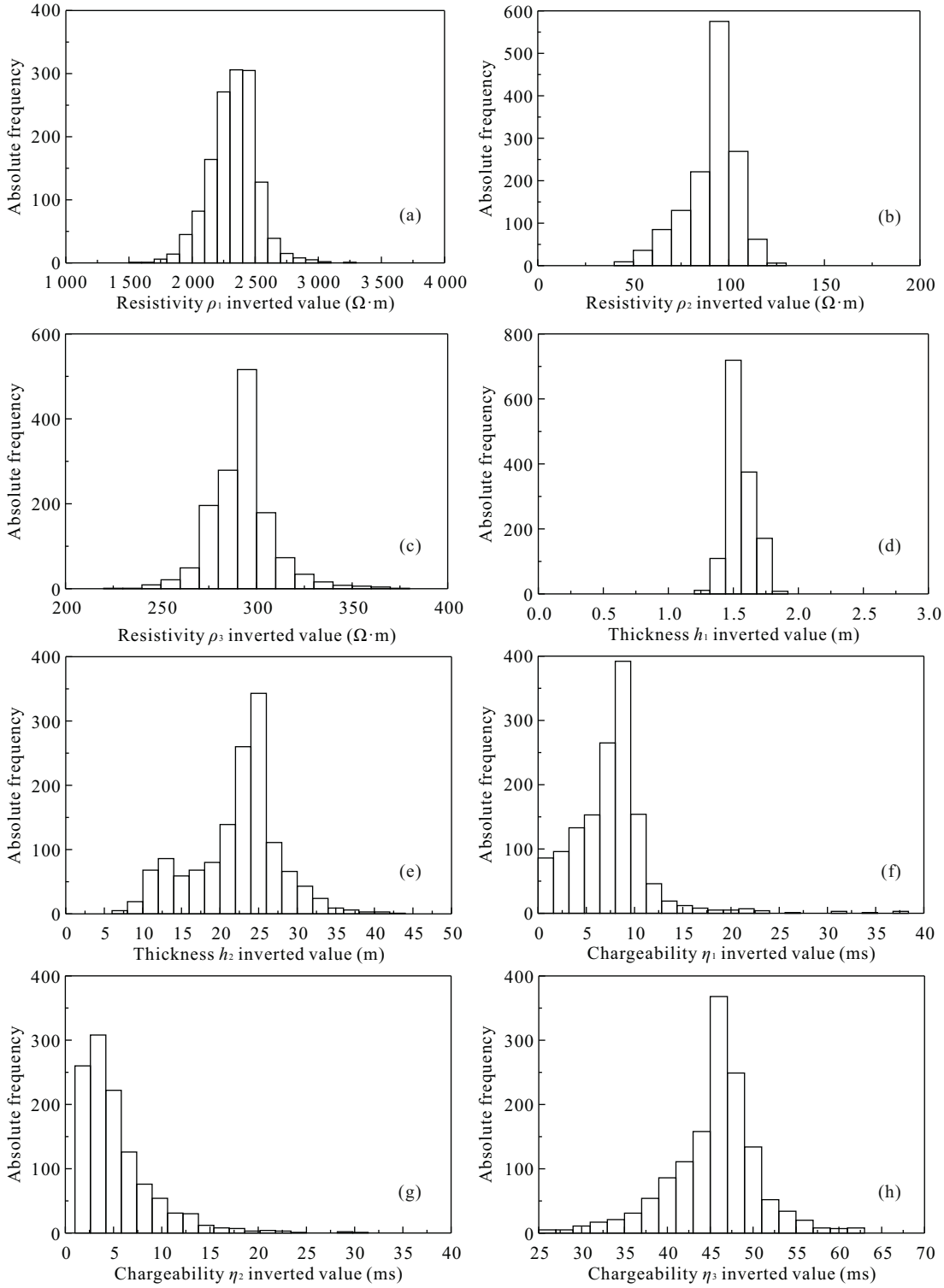

Figure 6. Histogram of inverted values ρ_1 (a), ρ_2 (b), ρ_3 (c), h_1 (d), h_2 (e), η_1 (f), η_2 (g), and η_3 (h) from Si-PSO inversion.

suitable to invert the VES data. Even if a very large search space is adopted, both the Se-PSO and Si-PSO inversion can effectively invert combined resistivity and IP data with high accuracy and convergence speed. So, the proposed Se-PSO or Si-PSO algorithm is a good selection to invert field data in cases where priori information is insufficient or even not available. As an approximate importance sampler, the CP-PSO based inverse algorithm can give evaluation by its posterior sampling. The posterior probability distributions show Si-PSO has more exploratory capability to search the model space more completely. That makes Si-PSO algorithm has an advantage over Se-PSO while inverting the VES data. Furthermore, Si-PSO algorithm can avoid a problem that the inversion accuracy of IP data depends heavily on the accuracy of inversion of the resistivity data due to sequentially operation in Se-PSO algorithm. Tests show that both Se-PSO and Si-PSO inversion algorithms are effective, robust, and easy to implement. In addition, PSO based inverse algorithm can perform a good posterior sampling of the equivalence region.

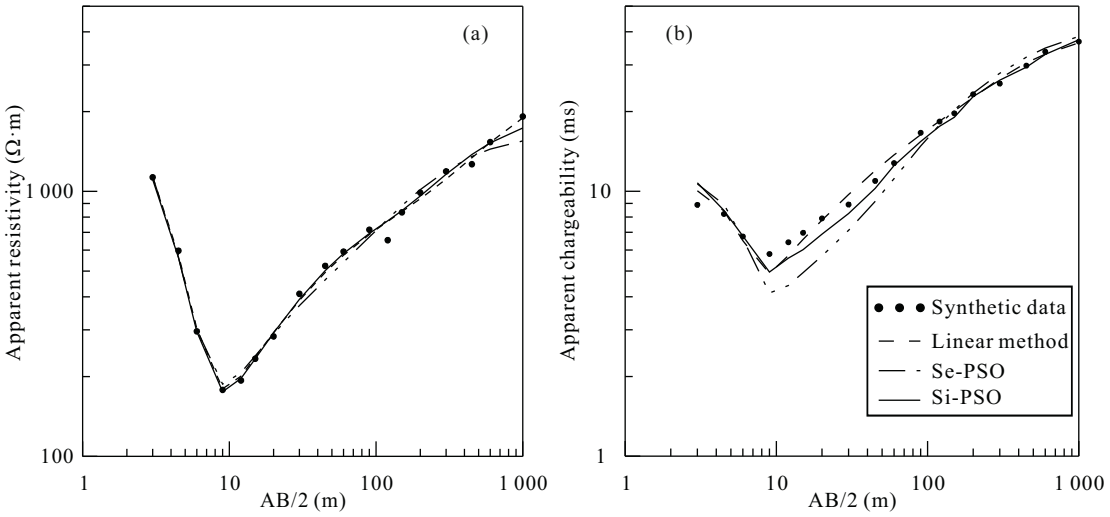

Figure 7. Match between synthetic data and the predicted data from 5-layered model. (a) The predicted resistivity data from models estimated from inversions using linear method, Se-PSO, and Si-PSO. (b) The predicted chargeability data from models estimated from inversions using linear method, Se-PSO, and Si-PSO.

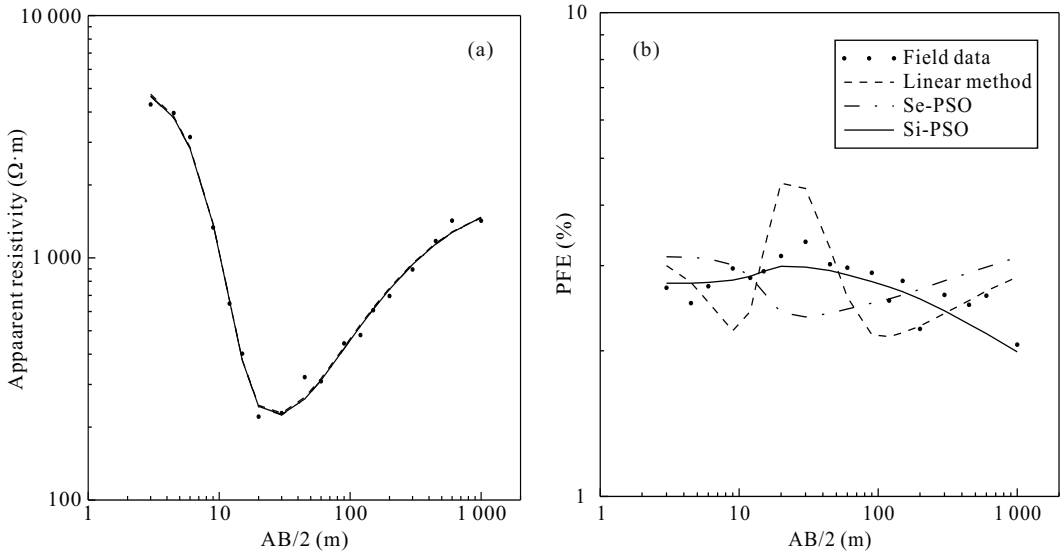

Figure 8. Resistivity and PFE match between field data and predicted data from model estimated by inversion. (a) Resistivity match; (b) PFE match.

These advantages make PSO is a powerful technique to invert different kinds of data simultaneously for the geophysical problems. Furthermore, there are also some future works arising from these studies, including more thoroughly algorithm complexity analysis and more field data tests.

ACKNOWLEDGMENTS

This work is supported by the National Natural Science Foundation of China (No. 41574123). We greatly appreciate Dr. Dai for providing us with his recently acquired field data from Africa. We also acknowledge the anonymous reviewers and editors for careful review of our manuscript and providing us with their comments and suggestion to improve the quality of the manuscript. The final publication is available at Springer via http://dx.doi.org/10.1007/s12583-017-0749-1.

REFERENCES CITED

Atekwana, E. A., Aal, G. Z. A., 2015. Iron Biomineralization Controls on Geophysical Signatures of Hydrocarbon Contaminated Sediments. *Journal of Earth Science*, 26(6): 835–843. doi:10.1007/s12583-015-0611-2

Chandra, S., Dewandel, B., Dutta, S., et al., 2010. Geophysical Model of Geological Discontinuities in a Granitic Aquifer: Analyzing Small Scale Variability of Electrical Resistivity for Groundwater Occurrences. *Journal of Applied Geophysics*, 71(4): 137–148. doi:10.1016/j.jappgeo.2010.06.003

Clerc, M. A., Kennedy, J., 2002. The Particle Swarm-Explosion, Stability, and Convergence in a Multi-Dimensional Complex Space. *IEEE Transactions on Evolutionary Computation*, 6(1): 58–73. doi:10.1109/4235.985692

Cui, Y. A., Zhu, X. X., Chen, Z. X., et al., 2016. Performance Evaluation for Intelligent Optimization Algorithms in Self-Potential Data Inversion. *Journal of Central South University*, 23(10): 2659–2668. doi:10.1007/s11771-016-3327-2

Fernández-Martínez, J. L., García-Gonzalo, E., Naudet, V., 2010a. Particle Swarm Optimization Applied to Solving and Appraising the Streaming-Potential Inverse Problem. *Geophysics*, 75(4): WA3–WA15. doi:10.1190/1.3460842

Fernández-Martínez, J. L., García-Gonzalo, E., Fernández-Álvarez, J. P., et

al., 2010b. PSO: A Powerful Algorithm to Solve Geophysical Inverse Problems Application to a 1D-DC Resistivity Case. *Journal of Applied Geophysics*, 71(1): 13–25

Fernández-Martínez, J. L., Mukerji, T., García-Gonzalo, E., et al., 2012. Reservoir Characterization and Inversion Uncertainty via a Family of Particle Swarm Optimizers. *Geophysics*, 77(1): M1–M16. doi:10.1190/geo2011-0041.1

Fernández-Martínez, J. L., Fernández-Álvarez, J. P., García-Gonzalo, E., et al., 2008. Particle Swarm Optimization (PSO): A Simple and Powerful Algorithm Family for Geophysical Inversion. *SEG*, *Expanded Abstracts*, 27(1): 3568–3571. doi:10.1190/1.3064068

Fernández-Martínez, J. L., García-Gonzalo, E., 2009. The PSO Family: Deduction, Stochastic Analysis and Comparison. *Swarm Intelligence*, 3(4): 245–273. doi:10.1007/s11721-009-0034-8

Gallas, J. D. F., Taioli, F., Filho, W. M., 2011. Induced Polarization, Resistivity, and Self-Potential: A Case History of Contamination Evaluation Due to Landfill Leakage. *Environmental Earth Sciences*, 63(2): 251–261. doi:10.1007/s12665-010-0696-y

Johnson, T. C., Versteeg, R. J., Ward, A., et al., 2010. Improved Hydrogeophysical Characterization and Monitoring through Parallel Modeling and Inversion of Time-Domain Resistivity and Induced-Polarization Data. *Geophysics*, 75(4): WA27–WA41. doi:10.1190/1.3475513

Kennedy, J., Eberhart, R., 1995. Particle Swarm Optimization. Proceedings of ICNN'95—International Conference on Neural Networks. IEEE Service Center, Piscataway, NJ. 1942–1948. doi:10.1109/icnn.1995.488968

Koefoed, O., 1979. Geosounding Principles. Elsevier Scientific Publishing Company, Amsterdam

Masson, F., Mouyen, M., Hwang, C., et al., 2012. Lithospheric Structure of Taiwan from Gravity Modelling and Sequential Inversion of Seismological and Gravity Data. *Tectonophysics*, 578: 3–9. doi:10.1016/j.tecto.2012.04.012

Pekşen, E., Yas, T., Kayman, A. Y., et al., 2011. Application of Particle Swarm Optimization on Self-Potential Data. *Journal of Applied Geophysics*, 75(2): 305–318. doi:10.1016/j.jappgeo.2011.07.013

Niwas, S., Gupta, P. K., 2011. Combined Straightforward Inversion of Resistivity and Induced Polarization (Time-Domain) Sounding Data. *Journal of Applied Geophysics*, 75(2): 319–326. doi:10.1016/j.jappgeo.2011.06.024

Santos, F. A. M., El-Kaliouby, H. M., 2010. Comparative Study of Local Versus Global Methods for 1D Joint Inversion of Direct Current Resistivity and Time-Domain Electromagnetic Data. *Near Surface Geophysics*, 8(2): 135–143. doi:10.3997/1873-0604.2009056

Santos, F. A. M., 2010. Inversion of Self-Potential of Idealized Bodies' Anomalies Using Particle Swarm Optimization. *Computers & Geosciences*, 36(9): 1185–1190. doi:10.1016/j.cageo.2010.01.011

Seigel, H. O., 1959. Mathematical Formulation and Type Curves for Induced Polarization. *Geophysics*, 24(3): 547–565. doi:10.1190/1.1438625

Sen Mrinal, K., Stoffa, P. L., 2013. Global Optimization Methods in Geophysical Inversion (2nd Edition). Cambridge University Press, Cambridge

Shaw, R., Srivastava, S., 2007. Particle Swarm Optimization: A New Tool to Invert Geophysical Data. *Geophysics*, 72(2): F75–F83. doi:10.1190/1.2432481

Song, X. H., Tang, L., Lü, X. C., et al., 2012. Application of Particle Swarm Optimization to Interpret Rayleigh Wave Dispersion Curves. *Journal of Applied Geophysics*, 84: 1–13. doi:10.1016/j.jappgeo.2012.05.011

Tang, J. T., Wang, F. Y., Xiao, X., et al., 2011. 2.5-D DC Resistivity Modeling Considering Flexibility and Accuracy. *Journal of Earth Science*, 22(1): 124–130. doi:10.1007/s12583-011-0163-z

Trelea, I. C., 2003. The Particle Swarm Optimization Algorithm: Convergence Analysis and Parameter Selection. *Information Processing Letters*, 85(6): 317–325. doi:10.1016/s0020-0190(02)00447-7

Veeken, P. C., Legeydo, P. J., Davidenko, Y. A., et al., 2009. Benefits of the Induced Polarization Geoelectric Method to Hydrocarbon Exploration. *Geophysics*, 74(2): B47–B59. doi:10.1190/1.3076607

Ye, Y. X., Hu, X. Y., Xu, D., 2015. A Goal-Oriented Adaptive Finite Element Method for 3D Resistivity Modeling Using Dual-Error Weighting Approach. *Journal of Earth Science*, 26(6): 821–826. doi:10.1007/s12583-015-0598-8

Zhu, J. F., Currens, J. C., Dinger, J. S., 2011. Challenges of Using Electrical Resistivity Method to Locate Karst Conduits—A Field Case in the Inner Bluegrass Region, Kentucky. *Journal of Applied Geophysics*, 75(3): 523–530. doi:10.1016/j.jappgeo.2011.08.009